Earth`s Cryosphere, 2019, vol. XXIII, No. 3, pp. 27–42 **http://earthcryosphere.ru/**

DOI: 10.21782/EC2541-9994-2019-3(27-42)

MODELING THE EVOLUTION OF MOUNTAIN GLACIERS: A CASE STUDY OF SARY-TOR GLACIER, INNER TIEN SHAN

O.O. Rybak[1–3], E.A. Rybak[1,2], N.A. Yaitskaya[1,2], V.V. Popovnin[4], I.I. Lavrentiev[5], R. Satylkanov[6], B. Zhakeyev[7]

[1]*Sochi Research Center, RAS, 8a, Theatralnaya str., Sochi, 354000, Russia; o.o.rybak@gmail.com*
[2]*Institute of Natural and Technical Systems, Sochi Branch, 99/18, Kurortny ave., Sochi, 354024, Russia*
[3]*Earth System Sciences and Department of Geography, Vrije Universiteit Brussel, 2, Pleinlaan, B-1050, Brussels, Belgium*
[4]*Lomonosov Moscow State University, Faculty of Geography, 1, Leninskie Gory, Moscow, 119991, Russia*
[5]*Institute of Geography, RAS, 29, Staromonetny per., Moscow, 119017, Russia*
[6]*Institute of Water Problems and Hydropower, Tien Shan Science Center, NAS KR, 9, Chikayeva str., Kyzyl-Suu, 722400, Issyk-Kul Region, Kyrgyz Republic*
[7]*Institute of Water Problems and Hydropower NAS KR, 533, Frunze str., Bishkek, 720033, Kyrgyz Republic*

In the paper, we consider evolution of Sary-Tor Glacier, Ak-Shiyrak Massif, Inner Tien Shan under changing climatic conditions. We describe in necessary detail structure of the model and set-up of the numerical experiments. For calibration and validation of the model we use results of measurements in snow pits and on ablation stakes in 2014–2016. A series of ten prognostic numerical experiments of 90 model years duration was performed. As a climatic forcing, we used air temperature and precipitation records on the weather station Tien-Shan–Kumtor located in the vicinity of the glacier. In the schematic scenarios, average daily surface air temperature grows with gradients 0–4 °C/100 years. Present-day glacier configuration is in imbalance with the climate of 2014–2016. As a result, area and volume of the glacier proceed to decrease until equilibrium is achieved after several tens of model years. Under extreme rates of temperature increase (+4 °C/100 years), Sary-Tor almost diminishes by the end of experiments. Glacial run-off rapidly decreases after initial growth in the first half of the experiments. Mathematical model inevitably contains simplifications of the real natural conditions. Nevertheless, obtained results will be useful in prognostic water balance calculations.

Mountain glacier, mass balance, climate, climate change, mathematical model, numerical experiment, Sary-Tor, Tien Shan

INTRODUCTION

Decline of mountain glaciers in Central Asia has been largely discussed in the scientific community for several past decades. Having both local and global importance, various aspects the problem have attracted international attention [*Bolch, 2007; Hagg et al., 2008; Kutuzov and Shahgedanova, 2009; Duyrgerov, 2010; Sorg et al., 2012; Petrakov et al., 2016*]. The surface mass balance of some glaciers has been modeled using recent observations [*Kronenberg et al., 2016; Kenzhebaev et al., 2017; Barandun et al., 2018*]. Mountain glaciers accumulate large amounts of fresh water which is a valuable resource for economy and social life of almost all states of this politically unstable region. As a consequence of reduction in atmospheric precipitation and glacier runoff expected by the end of the 21st century, the region may face drinking water shortage in the medium and remote perspective [*Bernauer and Siegfried, 2012; Siegfried et al., 2012*]. The concern about the current and future glacier shrinking is reasonable as the rivers originating in the Tien Shan provide water for about 100 million of people [*Aizen et al., 2007*]. The latter figure may seem overestimated, but the population only in the drainage basin of the Syr Dariya river (known as Naryn in the upper reaches) approaches 20,000,000 [*Bernauer and Siegfried, 2012*]. The population grows at high rates and may have been even larger after a few years after the year of cited publication [*Siegfried et al., 2012*].

Climate change affects fresh water availability and may cause floods, landslidings, droughts, and other natural hazards [*Ibatullin et al., 2009*]. Rapid melting of glaciers creates energy and food supply risks menacing sustainable development of the region [*Baetov and Arkhangelskaya, 2015*]. The glacier contraction problem becomes clearer when viewed in terms of meltwater contribution to the total runoff in High Mountain Asia, which may differ from one river basin to another. It exceeds 40 % of the annual runoff in the Indus upper reaches but is only 11.5 % for Ganges [*Lutz et al., 2014*]. Glaciers in Tajikistan provide 10–20 % of the annual discharge of large rivers but their contribution may increase to 70 % in hot and dry years [*Ibatullin et al., 2009*]. The pattern is similar in Kyrgyzstan, where meltwater from glaciers makes up to 50 % of mean annual runoff, and its input

The English text is published as edited by the authors.

reaches 70 % in the summer months (Fig. 4 in [*Sorg et al., 2012*]). The runoff provides water for agriculture, as well as for power production which covers up to 90 % of energy demands in the country [*Ibatullin et al., 2009*]. The power potential of 252 large and medium rivers in Kyrgyzstan exceeds $142 \cdot 10^9$ kW·h and is sufficient to meet the domestic and export demand. The catchment of the Naryn River, with a mean annual discharge of $(10–14) \cdot 10^9$ m^3, has the greatest potential [*Baetov and Arkhangelskaya, 2015*]. The Big Naryn and the whole river system source from the Kumtor River that originates in the Ak-Shyirak massif. Thus, the state of the Ak-Shyirak glaciers is of social and economic significance for the life of Kyrgyzstan in the changing world.

Forecast of water resources depend on correct prediction of glacial runoff. Dynamic projections are impossible for all glaciers in the Ak-Shyirak area because of the lack of observations and large computational cost, therefore, it is reasonable to model the evolution of selected glaciers. Recent projections of changes in glaciation and glacial runoff in major mountain systems of the Earth [*Huss and Hock, 2018b*], which are undoubtedly important for understanding possible responses of the Earth's cryosphere to climate change, were made using a simplified model, without consideration of some key factors, such as the effect of supraglacial moraines on the external heat exchange of glaciers.

The workflow for prognostic estimates of glacier runoff consists of several steps:

(1) choosing best documented reference glacier(s);

(2) choosing the type of model for best description of its (their) dynamics;

(3) tuning the chosen model by

– calibration against most probable values of key variables estimated with reference to available data on mass balance components and dynamics of the glacier(s);

– validation: reproducing in numerical experiment a set of observed values (flow velocity, mass balance, etc.) from input climate data;

(4) elaboration of a scenario of projected climate change, either as a schematic one [*Rets et al., 2011*] or based on global and/or regional modeling [*Morozova and Rybak, 2017*];

(5) running one or several numerical experiment(s) and interpreting its (their) results;

(6) choosing the method for extrapolating experimental results obtained for reference glaciers to other selected glaciers in the study region.

This study includes steps 1–5, with a special focus on methodological issues. The calculations are limited to the glacier response to changes in surface air temperatures assuming invariable precipitation patterns.

CHOICE OF A REFERENCE GLACIER

Sary-Tor glacier (41°50′ N, 78°11′ E) located at 3850–4780 m above sea level (asl) in Ak-Shyirak massif near the source of the Kumtor River is one of best studied glaciers in Kyrgyzstan (Fig. 1). The whole set of initial information necessary for modelling is available for this glacier (digital elevation

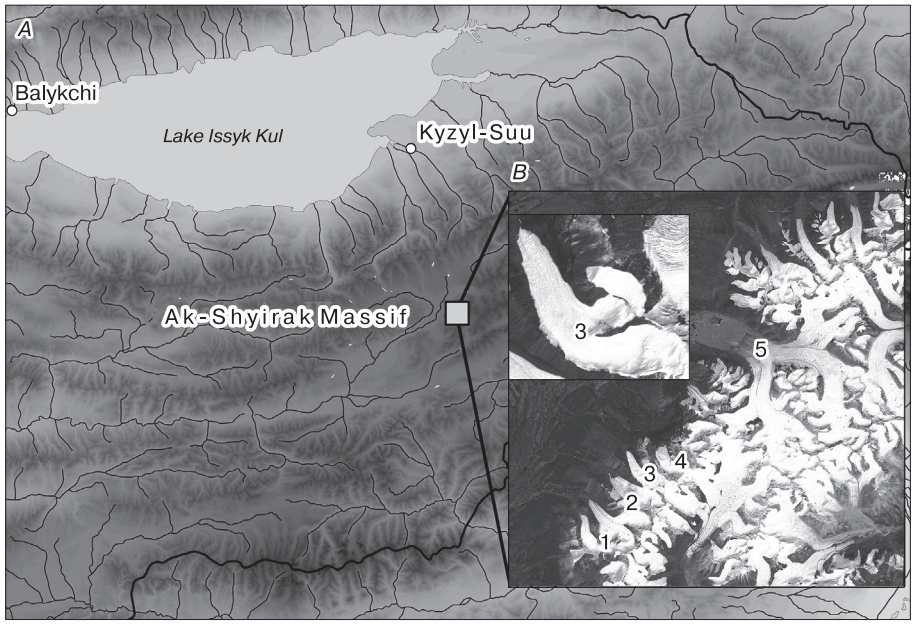

Fig. 1. Study area.

A: Ak-Shyirak Massif in the Inner Tien Shan, Kyrgyzstan; *B*: Sary-Tor glacier in Ak-Shyirak Massif. Numerals stand for names of glaciers: 1 = No. 354, 2 = Bordu, 3 = Sary-Tor, 4 = Davydov, 5 = Petrov.

model, map of ice thickness, climatic variables, etc.). Regular mass balance observations were carried out here in 1980s [*Ushnurtsev, 1991*] and have been resumed in 2014 after a long break. Sary-Tor glacier was characterized in detail by e.g. *Petrakov et al.* [*2014*]. The mass balance studies of glacier and its dependence on the regional climate began 30–40 years ago [*Duyrgerov and Ushnurtsev, 1988; Kuzmichenok, 1988; Duyrgerov et al., 1991, 1992; Ushnurtsev, 1991*]. For this reason, Sary-Tor is the most suitable among all glaciers in Ak-Shyirak massif to study runoff response to climate change, though mass balance observations and modeling were undertaken recently at the neighbor glacier No. 354 (Fig. 1) [*Barandun et al., 2018*]. Sary-Tor can be thought of as a kind of a reference glacier, and data about changes in its characteristics can be extrapolated to other Ak-Shyirak glaciers [*Mikhalenko, 1993*] to retrieve implicit evidence for glacier runoff changes.

MODELING

Choice of model type

The choice of the model type was based on its designation for projecting the response of the glacier to climate change, provided that the glacier is out of equilibrium with the present climate. The geometry of the glacier will obviously change in coming decades and application of pure mass balance models designed for local glaciers and neglecting prognostic geometry calculations [*Kronenberg et al., 2016; Kenzhebaev et al., 2017; Barandun et al., 2018*], will not allow evaluation future change in mass balance components. Using a simplified ice dynamics description [*Huss and Hock, 2018a,b*] coupled to a mass balance model appears to be an efficient approach to large-scale projections of glacier change in large mountain systems. However, such models are not accurate enough on the scale of individual glaciers. On the other hand, the sophisticated description of glacier dynamics in terms of the Full Stokes model requires large computational resources. A compromise solution would be to calculate the flow velocity using an "incomplete second order" model [*Pattyn, 2003*] that accounts for higher-order stress gradients neglected in the approach of *Huss and Hock* [*2018a*] but is simpler in implementation compared to the Full Stokes model. A similar model was applied to study the evolution of Morteratsch glacier in Switzerland [*Zekollari et al., 2014*] and Hans Tausen Iskappe ice dome in Greenland [*Zekollari et al., 2017*].

General model structure

The model of a mountain glacier dynamics consists of five units (Fig. 2): data input (1) and output (5) and units for calculations (2–4) of climate forcing (2), mass balance (3), and ice dynamics (4); each unit may comprise several subunits. The code is written in *FORTRAN90/95*, with program units corresponding to those of the model. Basic modeling approaches and algorithms were described earlier [*Oerlemans, 2001; Nemec et al., 2009; Fürst et al., 2011; Rybak et al., 2015*] but some are presented below for better understanding.

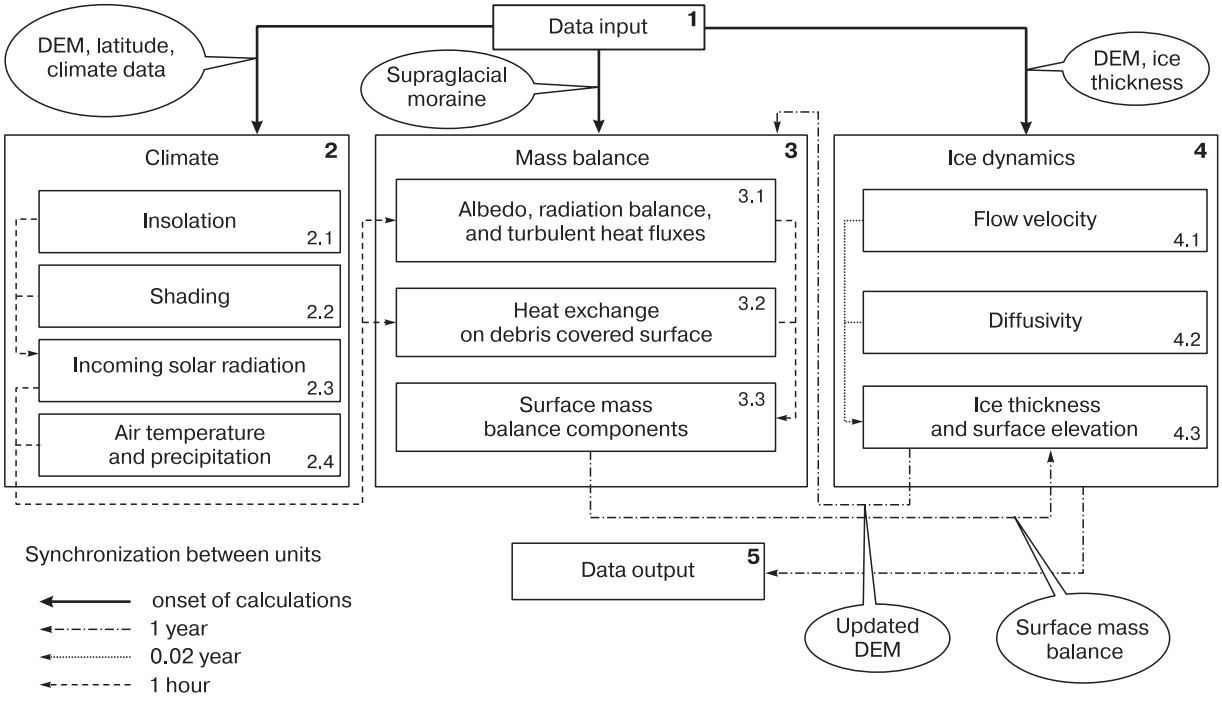

Fig. 2. Schematic representation of a mathematical model DEM = digital elevation model.

Climate

The algorithms for climate and mass-balance modeling originate from the idea of energy balance on the glacier surface which is related to the surface mass balance via energy available for melting [*Oerlemans, 2001; Nemec et al., 2009*]. The climatic block consists of four structural sub-units: calculation of incoming solar radiation on the top of the atmosphere at 1 h time step according to the algorithm of *Oke* [*1987*] (2.1); attribution of grid points shaded by surrounding relief depending on exposure (slope and azimuth, illumination angle, etc.) [*Dozier and Frew, 1990*] (2.2); calculation of incoming short-wave radiation flux to the horizontal surface (2.3); and air temperatures and precipitation (2.4). The short-wave radiation flux is estimated using results of (2.1) and (2.2), as well as the transmissivity of the atmosphere (κ_a):

$$SW = \kappa_a S_0 = (\kappa_0 + \theta z) S_0,$$

where S_0 is the solar constant (solar irradiance per time unit per unit area, on a surface perpendicular to solar rays, outside of the Earth's atmosphere at the average distance of the Earth from the Sun [*Kondratiev, 1965*]); κ_a depends on absolute elevation z; $\theta = 6 \cdot 10^{-5}$ m^{-1} is the empirical constant; $\kappa_0 = 0.6$. The short-wave radiation SW consists of direct and diffuse components: $SW = Q_{dir} + Q_{dif}$ which, in turn, are calculated dependently on the cloud cover ($\bar{c}$):

$$Q_{dir} = (1 - \bar{c}) \delta f_{dir} SW \kappa \sin(h_S + \gamma_S),$$

$$Q_{dif} = f_{dif} SW \kappa \sin(h_S),$$

where h_S is the Sun height; γ_S is the angle between the glacier surface and the horizontal sun projection:

$$\gamma_S = \mathrm{tg}\left[\varphi \cos(a - \xi)\right],$$

where φ is the glacier surface slope; a is the current solar azimuth dependent on geographical coordinates and time of the day; ξ is the orientation of the glacier surface; f_{dir} and f_{dif} are conventional shares of direct and diffuse radiation in the total incoming radiation, which have multiple controls; $\delta = 1$ or $\delta = 0$ in case of absence or presence of shading from surrounding mountains at the respective grid point (2.2).

The fields of air temperature and precipitation (2.4) are calculated on the basis of the input climate data (unit 1). Dependently on the problem, these can be either observations on the nearest weather stations close to the glacier [*Rybak and Rybak, 2017*], or results of prognostic calculations downscaled to the scale of a particular glacier [*Morozova and Rybak, 2017*], or both.

We do not know, how the air temperature is distributed above the glacier. That is why, in order to calculate mean daily surface air temperature field (T_A), we applied constant vertical temperature lapse rate (γ) and temperature shift (ΔT).

This approach appears more reasonable than applying average or characteristic values which are unsuitable because both γ and ΔT may vary even within a single glacier [*Voloshina, 2002*]. Therefore, we consider γ and ΔT as tuning parameters:

$$\bar{T}_A = T_t + \gamma z + \Delta T,$$

where T_t is the mean daily air temperature at a regular weather station.

Since all calculations in the climatic block are performed at a 1 h time step, surface air temperature is evaluated every hour using a simple harmonic function

$$T_A = \bar{T}_A - \tilde{T}_A \cos\left(2\pi \frac{t}{24}\right), \qquad (1)$$

where $\tilde{T}_A$ is the daily temperature amplitude; $t = 0, ..., 23$ is time, h. Although the real air temperature variations may deviate from the harmonic behavior, using equation (1) is more reasonable than complicated derivation for T_A in prognostic calculations. The key adjustable parameter $\tilde{T}_A$ is found according to observations. Its value is especially important during ablation season.

The similar approach was used to get the series of daily precipitation sums P_t averaged by balance years (apparently, in contrast to temperature, every day summation was used instead of averaging). The fraction of solid precipitation P_S depends on air temperature: $P_S = P \cdot f(T)$, where f is a sine function of temperature [*Robinson et al., 2010*] in the range from –2 to 2 °C; $f = 1$ at $T_A \leqslant -2$ °C (only snow) and $f = 0$ at $T_A \geqslant 2$ °C (only rain). Precipitation was calculated at each grid point as

$$P = P_t + \gamma_P (z - z_0),$$

where γ_P is the precipitation elevation gradient found from field measurements; z is the elevation (m asl); z_0 is the elevation of the lowermost point of the glacier terminus (3850 m asl). As a result, the modeled distribution of precipitation corresponded to calculated accumulation above 4400 m asl where all precipitation is solid.

Mass balance

This model version does not include heat transfer in snow (firn) layer and inside the glacier. Heat exchange is calculated for an infinitely thin skin layer of surface ice. Its temperature T_S is assumed to be the same as surface air T_A temperature but cannot exceed the melting point T_0:

$$T_S = T_A, \quad T_A \leq T_0,$$
$$T_S = T_0, \quad T_A > T_0,$$

where $T_0 = 273.15$ K is the absolute water freezing temperature.

Air temperature over the glacier and, therefore, snow/ice temperature are given in the climatic unit (2). The surface temperature is used to calculate ef-

fective emissivity E_{eff} (3.1) using the Brunt formula corrected for the cloud cover:

$$E_{eff} = \sigma T_S^4 \left(a_1 + b_1 e^{1/2}\right)\left(1 - \overline{c}m\right), \quad (2)$$

where $\sigma = 5.67 \cdot 10^{-8}$ W/(m^2·K^4) is the Stefan–Boltzmann constant; $a_1 = 0.39$ and $b_1 = 0.05$ are the empirical constants; m is the cloud cover; $\overline{c} = 0.7$ ($P > 0$), $\overline{c} = 0.1$ ($P = 0$).

The partial pressure of water vapor e is assumed to be proportional to the atmospheric pressure and to the air water content q.

The surface albedo α is calculated as described in [*Nemec et al., 2009*]

$$\alpha = \alpha_s + \left(\alpha_s - \alpha_i\right)\exp\left(-d/d^*\right), \quad (3)$$

where $\alpha_s = 0.6$ is the characteristic snow albedo; $\alpha_i = 0.2$ is the characteristic ice albedo; d is the snow depth; $d^* = 0.5$ m is the characteristic snow depth.

The sensible and the latent turbulent heat flux components (*SHF* and *LHF*, respectively) over the snow/ice surface contribute little to the heat budget [*Golubev et al., 1978; Voloshina, 2002*] and are calculated in a simplified way for the ablation zone only, if $T_A > T_0$ [*Braithwaite and Olesen, 1990*]:

$$SHF = L_m K_S \left(T_A - T_0\right) vp / s_{day}; \quad (4)$$

$$LHF = L_m K_L \left(e - e_s\right) v / s_{day}, \quad (5)$$

where $L_m = 3.35 \cdot 10^5$ J/kg is the specific heat of melting; $K_S = 6.34 \cdot 10^{-6}$ kg·m^2/day over ice; $K_S = 4.42 \cdot 10^{-6}$ kg·m^2/day over snow; $K_L = 11.14 \cdot 10^{-3}$ kg·m^2/day over ice; $K_L = 7.77 \cdot 10^{-3}$ kg·m^2/day over snow; v is the wind speed modulus (adjustable parameter); p is the air pressure; e is the water vapor pressure; e_s is the saturation water vapor pressure (both variables are found for 70 % relative humidity); $s_{day} = 86\,400$ is the number of seconds in 24 hours. As follows from (4) and (5), *SHF* is always positive and *LHF* is always negative.

Equations (4) and (5) are inapplicable to glacier parts covered with supraglacial moraine, because turbulent fluxes significantly contribute here to heat exchange of the glacier with the atmosphere. However, debris covers a negligibly small part of Sary Tor glacier [*Petrakov et al., 2014*] and has no effect on its total surface mass balance. Therefore, step 3.2 is omitted in the current modeling version.

The energy balance consists of components defined by equations (2)–(5):

$$E = SW\left(1 - \alpha\right) - E_{eff} + SHF + LHF.$$

E refers to the amount of energy available for melting of snow/ice (M) and is a key variable in the mass balance calculations:

$$\begin{aligned} M &= \max\left(E, 0\right)/L_m, \quad T_S \geq T_0, \\ M &= 0, \qquad\qquad T_S < T_0. \end{aligned} \quad (6)$$

In this study, accumulation is calculated without several poorly constrained components: snow drift over the glacier; potential precipitation enhancement induced by micro-circulation; and avalanche feeding [*Rybak and Rybak, 2017*]. These contributions to the mass balance of the Sary Tor (and for the most of other glaciers) are unknown, except for some implicit estimates [*Voloshina, 2002*], while limited data available for other glaciers [*Popovnin and Pylaeva, 2015*] are specific to those ones implying no extrapolation.

The annual surface mass balance (*SMB*) of the glacier is found as difference between accumulation (*ACC*) and runoff (*RO*) per model year:

$$SMB = \sum_1^{365} \left[ACC - RO\right]. \quad (7)$$

Accumulation (*ACC*) is found as solid precipitation (*PS*) minus the amount of moisture evaporated from the surface (*SU*) proportional to the latent heat flux *LHF* (5):

$$ACC = PS - SU.$$

From (5) it follows that only liquid water (meltwater and liquid precipitation) can evaporate in the ablation zone. The glacial runoff consists of the mass M of melted snow and ice (equation (6)) minus the amount of refrozen water (*RF*).

The amount of refrozen water (*RF*) is limited by the mass of available water for freezing W_r, porosity of the snow/firn surface layer, and surface energy balance [*Reijmer et al., 2012*]. Liquid precipitation is excluded from the formal statement of the surface mass balance, that is why $W_r = M$. As an additional indicator, we calculate total runoff, which differs from the glacial runoff for the amount of water precipitated on the glaciated area. In future, this characteristic can be collated with water discharge measurements lower the glacier terminus.

In a simplified case, amount of refrozen water can be expressed as [*Janssens and Huybrechts, 2000*]

$$RF = \min\left[P_r, W_r\right],$$

where P_r is potentially retained meltwater, evaluated using formula of *Oerlemans* [*1991*] adapted for mountain glaciers:

$$P_r = \max\left(E, 0\right)\left[1 - C_{RF}^{T_S - T_0}\right]/L_m, \quad (8)$$

where $C_{RF} = 1.05$ is an adjustable coefficient. The approach of *Oerlemans* [*1991*] implies that the heat released by refreezing can be neglected in the energy balance calculations.

The meltwater is assumed to either refreeze during the same day when it melts or to escape from the snow/firn layer. Note that the original version of equation (8) uses an exponent instead of the C_{RF} coefficient and the average temperature of the upper 2 m of snow/firn layer instead of T_S. The algorithm of (8) is simple but quite efficient and yields results comparable with those of more sophisticated snow models [*Reijmer et al., 2012*].

Dynamics

Dynamical unit (4) is designated for calculation of flow velocity (4.1), nonlinear diffusion (4.2), and ice thickness (4.3). The theoretical background and algorithms were described previously [*Pattyn, 2003; Fürst et al., 2011; Rybak et al., 2015*], and here we confine ourselves to some most relevant issues. The horizontal components of flow velocity (u, v) are found by solving the system of nonlinear elliptic equations

$$\begin{aligned} &4\frac{\partial}{\partial x}\left(\eta\frac{\partial u}{\partial x}\right)+2\frac{\partial}{\partial x}\left(\eta\frac{\partial v}{\partial y}\right)+\frac{\partial}{\partial y}\left(\eta\frac{\partial u}{\partial y}\right)+\\ &+\frac{\partial}{\partial y}\left(\eta\frac{\partial v}{\partial x}\right)+\frac{\partial}{\partial z}\left(\eta\frac{\partial u}{\partial z}\right)=\rho_i g\frac{\partial s}{\partial x},\\ &4\frac{\partial}{\partial y}\left(\eta\frac{\partial v}{\partial y}\right)+2\frac{\partial}{\partial y}\left(\eta\frac{\partial u}{\partial x}\right)+\frac{\partial}{\partial x}\left(\eta\frac{\partial u}{\partial y}\right)+\\ &+\frac{\partial}{\partial x}\left(\eta\frac{\partial v}{\partial x}\right)+\frac{\partial}{\partial z}\left(\eta\frac{\partial v}{\partial z}\right)=\rho_i g\frac{\partial s}{\partial y}, \end{aligned} \tag{9}$$

where η is the effective viscosity,

$$\eta=\frac{1}{2}A(T)^{-1/n}\left[\left(\frac{\partial u}{\partial x}\right)^2+\left(\frac{\partial v}{\partial y}\right)^2+\frac{\partial u}{\partial x}\frac{\partial v}{\partial y}+\right.$$
$$\left.+\frac{1}{4}\left(\frac{\partial u}{\partial y}+\frac{\partial v}{\partial x}\right)^2+\frac{1}{4}\left(\frac{\partial u}{\partial z}\right)^2+\frac{1}{4}\left(\frac{\partial v}{\partial z}\right)^2\right]^{(1-n)/2n},$$

$A(T)$ is the rheological function dependent on ice temperature; s is the glacier surface elevation; ρ_i = = 910 kg/m^3 is the ice density; n = 3. The glacier is assumed to be isothermal, and the rheological function can be replaced by the parameter A_{fl}, though this may be not the case in reality. According to radio-echo sounding, Sary-Tor is a polythermal glacier composed of cold (<0 °C) ice in the upper part and of warm water-bearing ice near the base [*Petrakov et al., 2014*], which is prerequisite for basal sliding. The basal sliding velocity vector is assumed to be proportional to the basal drag (τ_b) in the third power:

$$\mathbf{v}\big|_b=-\mu\tau_b^3,$$

where μ is the friction coefficient; τ_{bx} and τ_{by} are the stress tensor components:

$$\tau_{bx}=\left[\tau_{xz}-\tau_{bxy}\frac{\partial b}{\partial y}-\left(2\tau_{xx}+\tau_{yy}\right)\frac{\partial b}{\partial x}\right]_b,$$
$$\tau_{by}=\left[\tau_{yz}-\tau_{bxy}\frac{\partial b}{\partial x}-\left(2\tau_{yy}+\tau_{xx}\right)\frac{\partial b}{\partial y}\right]_b,$$

b is the bedrock elevation; τ_{ij} are the stress tensor components at the glacier base.

Each equation in system (9) is solved by the conjugate gradient method, and the system itself is solved by the Picard iteration method using a relaxation scheme [*Rybak, 2011*].

Ice thickness (sub-unit 4.3) is found by solving the mass conservation equation written for local ice thickness H, where the surface mass balance (*SMB*) enters its right-hand side:

$$\frac{\partial H}{\partial t}=-\nabla\cdot\left(\mathbf{v}_h H\right)+SMB=-\nabla\cdot\left(D\nabla H\right)+SMB,$$

where t is time; $\mathbf{v}_h$ is the vertically averaged velocity vector; D is a nonlinear complex (nonlinear diffusion (sub-unit 4.2).

Equation (9) is solved numerically by the unconditionally stable alternating direction implicit (ADI) method. The nonlinear diffusion components D_x and D_y are expressed via flow velocity components, ice thickness, and slope of the glacier surface:

$$D_x=-uH\left(\frac{\partial s}{\partial x}\right)^{-1},\quad D_y=-vH\left(\frac{\partial s}{\partial y}\right)^{-1}.$$

Interaction between model units

The climate (2) and mass balance (3) units are run at a time step of 1 h. The results, after summation of daily data for one balance year, are used in calculations of ice dynamics (4). Adjustment of the velocity field to the ice thickness field at the specified *SMB* field (equation (7)) is carried out by small time steps of 0.02 yr. The updated field of the glacier surface elevation and glacier mask in grid cells by the end of each model year are used for updating the glacier surface orientation and vertical gradients of air temperatures and precipitation as well as mass balance to define the mass-balance modeling domain. Output of the results is carried out in the end of each balance year.

SET-UP OF NUMERICAL EXPERIMENTS

Input data

Mean daily air temperature T_A over the glacier was estimated from 3-hour standard-measurements at the Tien Shan–Kumtor weather station located few kilometers away from the glacier at 3675 m asl. The input data were averaged (surface air temperature T_t) or summated (precipitation P_t) over 24 h and also averaged over two balance years (2014/15; 2015/16) (Fig. 3).

The ice thickness field (Fig. 4) was reconstructed from radio-echo sounding performed in May, 2013. The glacier contours were obtained by deciphering a *Landsat* image of 2012 [*Petrakov et al., 2014*]. The calculation results were scaled to regular grid points (25 m spatial resolution), as well as elevations based on the ASTER GDEM, Version 2 digital elevation model [*ASTER..., 2011*] with the horizontal resolution of 30 m and the vertical accuracy of 12 m for mountain areas. The 4 × 3 km integration domain comprises the glacier itself and the surrounding mountains (to account for shading effect). The area in Figs. 4–7 is slightly smaller (3 × 2.75 km).

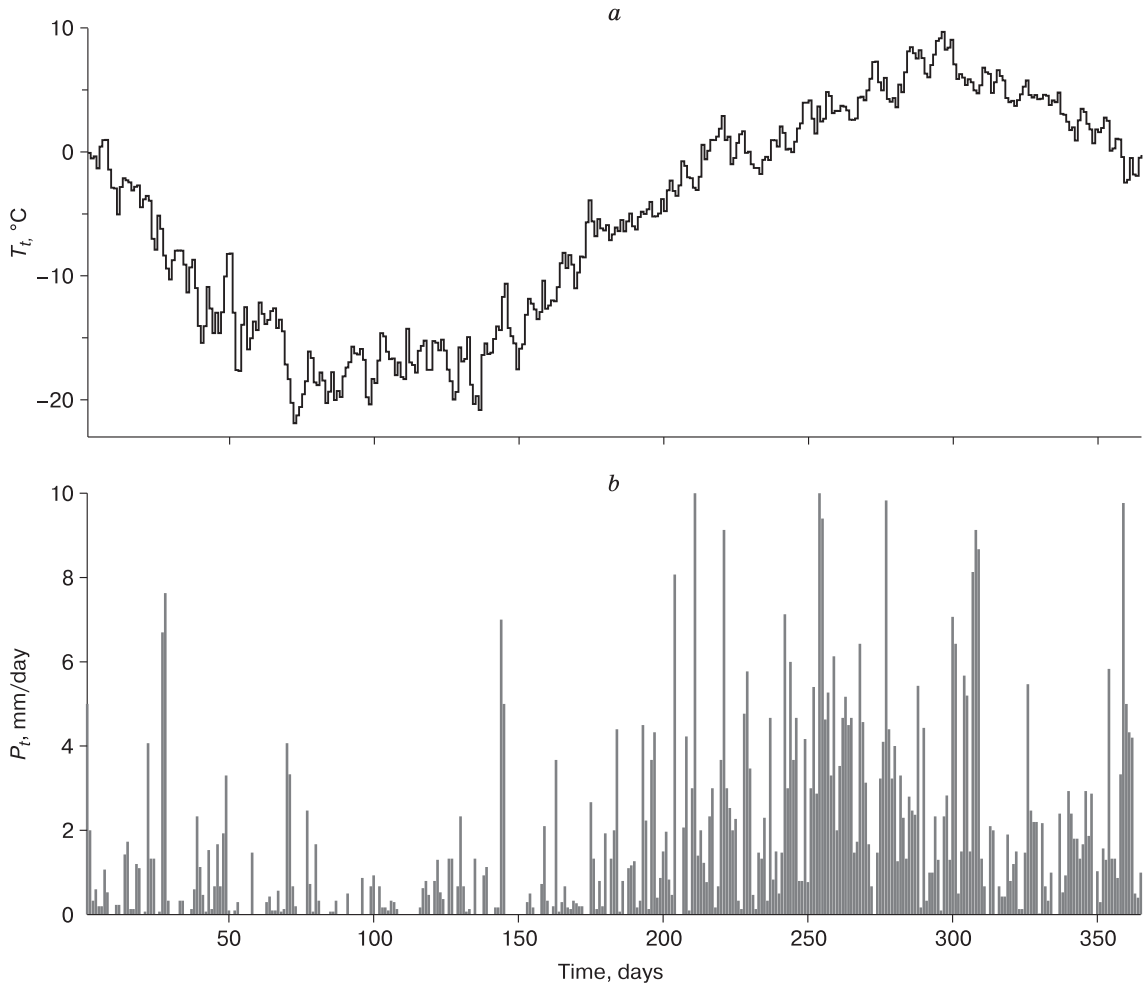

Fig. 3. Input climatic data, averaged over two hydrological years (2014/15, 2015/16).

a: mean daily surface air temperature, T_t, °C; *b*: daily sums of precipitation P_t, mm, Tien Shan weather station.

Numerical experiments

The computation was run in two series composed of three preliminary and ten main experiments (Table 1). Two preliminary experiments focused on ice dynamics (P1, P2) without climate and mass balance calculations and one experiment (P3) was for joint climate and mass balance modeling without calculations of ice dynamics. Constraining the contributions of A_{fl} and μ is challenging even for quite a large series of flow velocity data [*Zekollari et al., 2013*]. Currently, calibration of a dynamic model of Sary-Tor glacier is impossible since no field flow velocity observations are available. The experiments were run in two modes (Table 1): normal mode 1, with A_{fl} and μ similar to the values for Morteratsch (Switzerland) [*Zekollari et al., 2013*] and Marukh (Western Caucasus) glaciers [*Rybak et al., 2015*], and accelerated mode 2, with a higher deformational component of the flow velocity at the account of higher A_{fl} and a lower sliding component at lower μ.

Coupling of blocks in a full dynamic model allowed carrying out simulation of the glacier evolution in schematically imposed changing climatic conditions. The main series consisted of ten experiments of 90 model years duration each: five in the normal mode and five in the accelerated mode. The 2011/12 hydrological year was chosen as the first year of integration, when the topographic base was compiled using remote sensing satellite data (see above).

The climate and mass-balance obtained for 300 model years of integration without ice dynamics calculation (output of experiment P3) was taken as the initial condition. Two first experiments (E01, E02) were assumed as an apparent continuation of experiment P3, but with dynamic block activated. Results of these experiments reflected equilibrium state of the glacier with the climate of 2014–2016. Experiments E03–E10 were performed assuming 1–4 °C/100 yr warming rate (Table 1) at fixed precipitation rate.

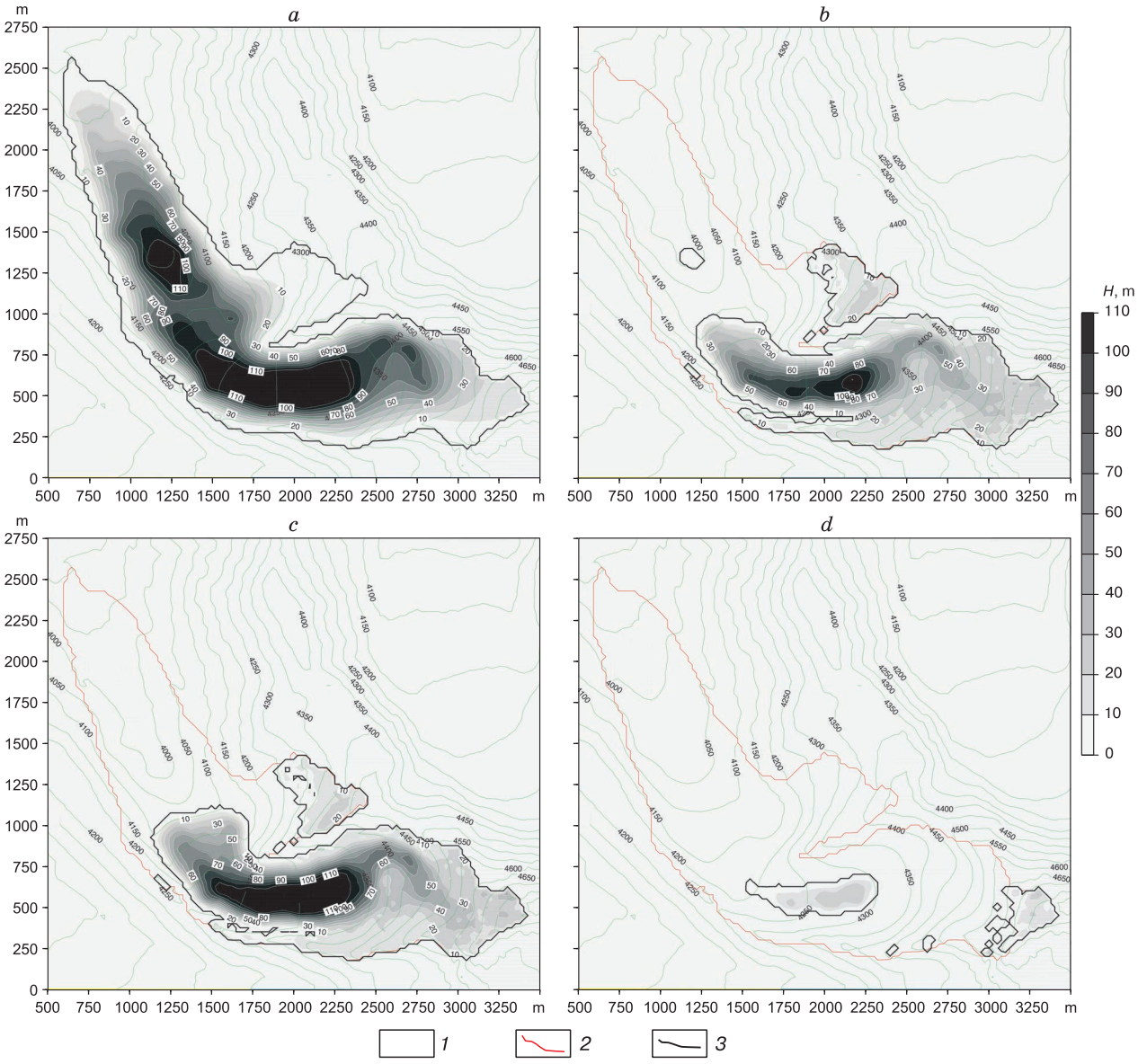

Fig. 4. Ice thickness (H) of Sary-Tor glacier.

a: measured; *b*–*d*: model values after 90 years of integration in experiments E01, E02, E10, respectively; *1* – isolines of altitude, m asl; *2* – initial glacier contours; *3* – glacier contours in the year 2100. Values on axes show distance from conventional zero point.

MODELING RESULTS AND DISCUSSION

Ice flow velocity (mass-balance block switched off)

The velocity of both surface (Fig. 5, *a*, *b*) and basal (Fig. 5, *c*, *d*) ice flow is the highest (>50 m/yr) in the area where steep slope is combined with high ice thickness (Fig. 4, *a*), between 4350 and 4450 m asl, as predicted in the mode 1 (Fig. 5, *a*). This area is somewhat larger when calculations are carried out in the mode 2 (Fig. 5, *b*). Another high-velocity area is located downstream in a flat zone, where ice thickness exceeds 110 m.

Mass balance components (dynamic block switched off)

Accumulation, ablation, and mass balance in 2014/15 and 2015/16 balance years were calculated basing on ablation measurements on stakes planted along the middle flowline of the glacier, snow depth surveys, and measurements in snow pits and at stationary precipitation gauges (run by the Institute of Water Problems and Hydro Power of the National Academy of Sciences of Kyrgyzstan in 2014–2016). Extrapolation of stake measurements from a sparse network onto the entire glacier territory may cause

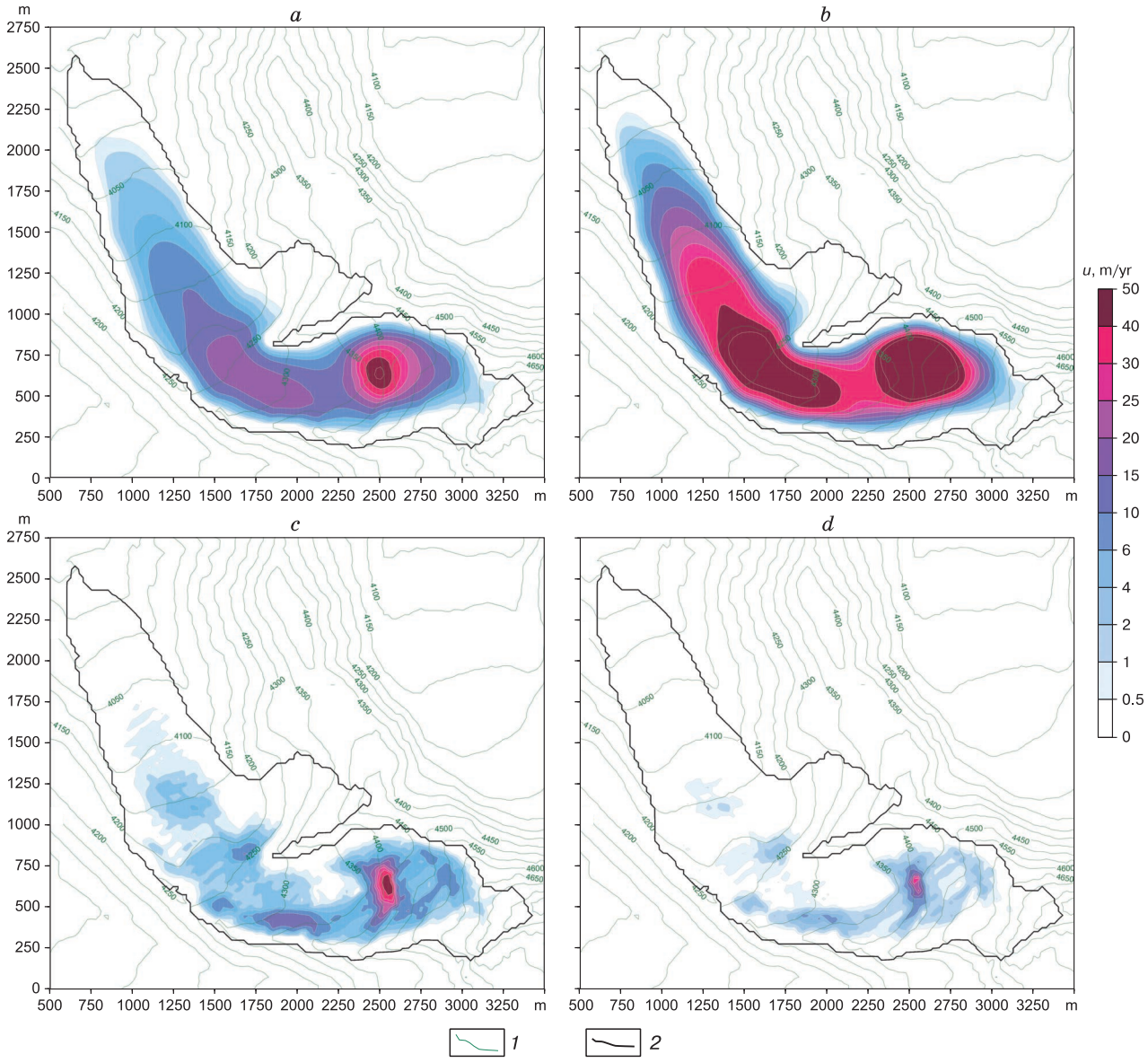

Fig. 5. Surface (*a*, *b*) and basal (*c*, *d*) ice flow velocities calculated prior to climate forcing in experiments P1 (*a*, *c*) and P2 (*b*, *d*).

1 – elevation contour lines (asl); *2* – initial glacier contours.

errors to ablation estimates and the respective specific mass balance. However, since no alternative was available, the model parameters were tuned to reproduce most correctly the fields of observed accumulation and the field of calculated surface mass balance averaged over two balance years, 2014/15 and 2015/16.

In the absence of ice flow in experiment P3, topography and ice thickness were fixed, and snow depth was the only characteristic that varied from year to year and controlled albedo and, therefore, surface mass balance components. At the specified values of tuned model parameters, the melt rate increased rapidly from 500 to 1070 mm/yr during the first 30 model years and then more slowly to 1270 mm/yr during the next 270 years; the increase was especially slow in the last 150 years, and almost zero by the 300-th year (Fig. 8). Surface mass balance, on the contrary, fell from low positive values (+80 mm/yr) to –550 mm/yr during the first 30 years and then decreased slowly during the next 270 years (to –743 mm/yr), at an almost zero rate by the 300-th year. The resulting steady-state fields are shown in Fig. 6: melting obviously affects the entire glacier

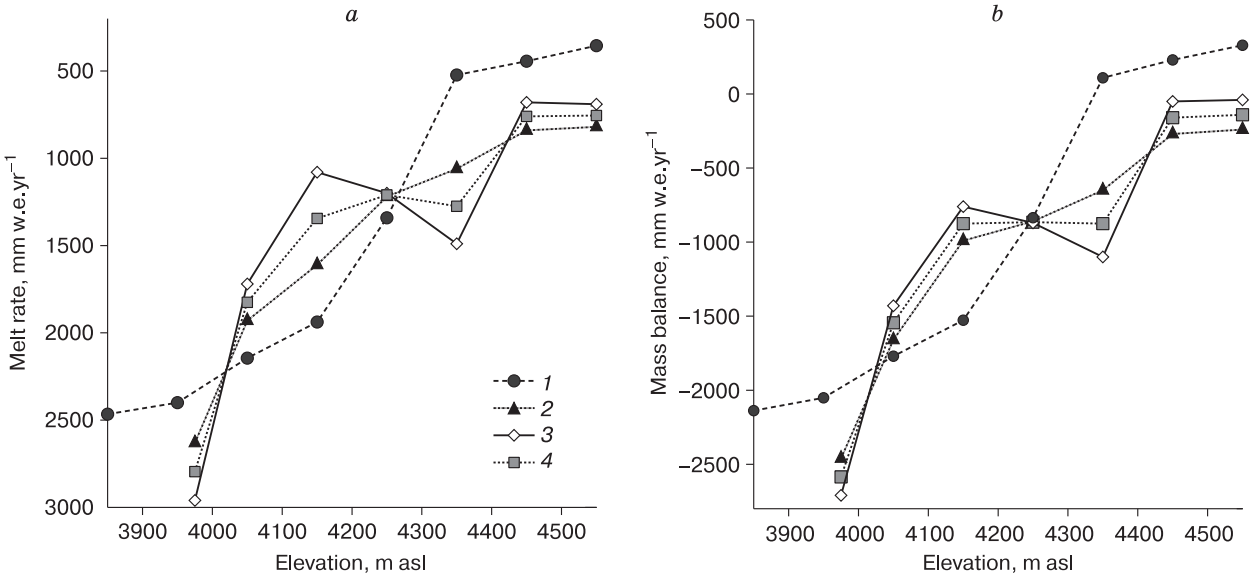

Fig. 6. Predicted and observed (inferred) melt rates (*a*) and surface mass balance (*b*) averaged over elevation zones.

1 – predicted; *2* – observed, 2014/15; *3* – observed, 2015/16; *4* – average over 2014–2016.

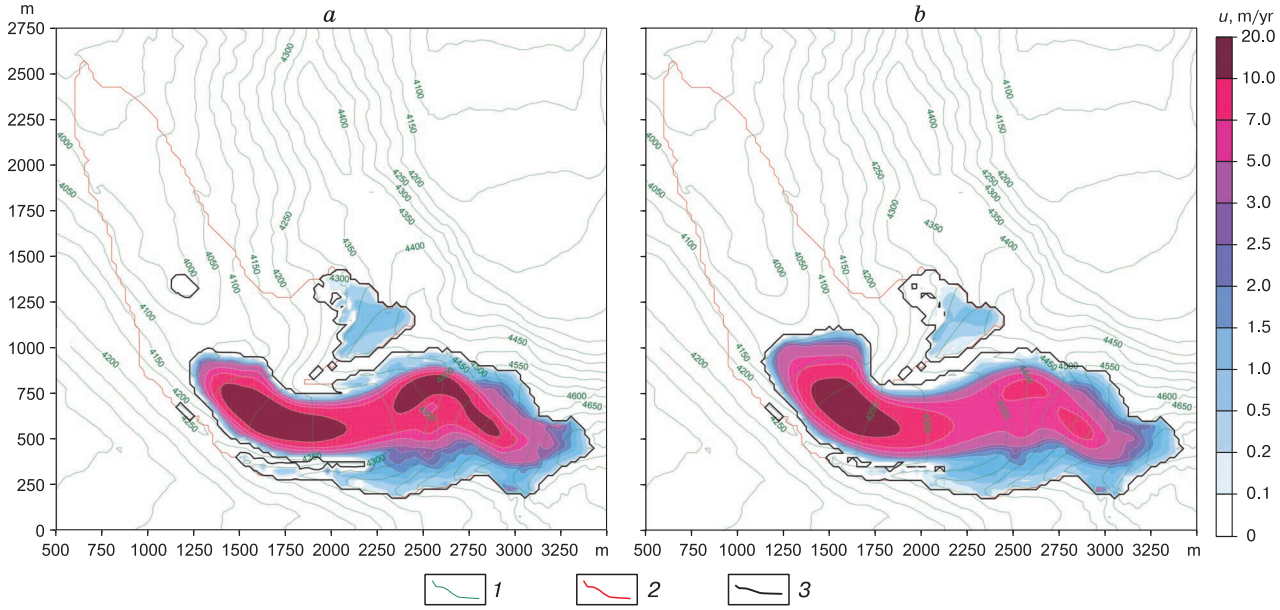

Fig. 7. Ice flow velocity on the glacier surface after 90 years of integration in experiments E01 (*a*) and E02 (*b*).

1 – isolines of altitude, m asl; *2* – initial glacier contours; *3* – glacier contours in the end of experiments.

area (Fig. 6, *a*), its duration decreases from 150–160 days at the glacier front to less than 80 days above 4650 m asl. The amount of meltwater decreases from 2600 mm/yr of water equivalent (w.e.) at the glacial front to less than 200 mm/yr above 4500 m asl (Fig. 6, *b*). The snow line is located at 4250–4350 m (Fig. 6, *c*).

Averages over the whole glacier were chosen as the target values for tuning the model (Table 2). This did not apparently mean strict identity in vertical distribution of the observed (reconstructed) and modeled characteristics. With a given set of tuning parameters, the model overestimated ablation over the whole glacier for 3.3 % and underestimated spe-

Table 1. **Numerical experiments**

No.	Name	Description	Characteristics	Mode	Temperature gradient, °C/100 yr
1	P1	Preliminary	No mass balance modeling	Mode 1	
2	P2	«	Same	Mode 2	
3	P3	«	No ice dynamics modeling		
4	E01	Main	All modeling options active	Mode 2	0
5	E02	«	Same	Mode 1	0
6	E03	«	«	Mode 2	+1
7	E04	«	«	Mode 1	+1
8	E05	«	«	Mode 2	+2
9	E06	«	«	Mode 1	+2
10	E07	«	«	Mode 2	+3
11	E08	«	«	Mode 1	+3
12	E09	«	«	Mode 2	+4
13	E10	«	«	Mode 1	+4

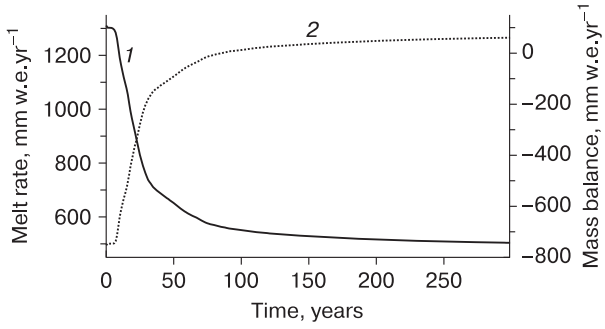

Fig. 8. Adjustment of ablation and specific mass balance to specified measured values in experiment with fixed surface topography.

1 – melt rate; *2* – mass balance.

Table 2. **Calculated and model values of accumulation, total melting, and specific mass balance for the Sary-Tor glacier**

Parameter	Calculated from field data			Predicted
	2014/15	2015/16	Averaged over 2014–2016	
Accumulation (4400–4500 m asl)	570	630	**600**	618
Accumulation (above 4500 m asl)	580	650	**615**	625
Total melting, mm w.e.	−1240	−1210	**−1225**	−1266
Mass balance, mm w.e.	−820	−790	**−805**	−743

Note: w.e. is water equivalent. Target values are in bold.

cific mass balance for 9.2 %. Comparison of values averaged over elevation zones (Fig. 9, *a*, *b*) shows that changes in gradients commensurate within 4050–4200 and above 4350 m. The calculations are generally closer to the measured data for 2014/15 than to those for 2015/16. Essential misfit appears above 4350 m, where the modelled mass balance is positive while that based on observations is negative (though slightly). It is unclear, what could be the reason for the positive melt rate gradient (and negative gradient in specific mass balance) in the elevation belt 4250–4350 m in 2015/16. Anyway, more longer time series of observations is required for the more accurate calibration of the mass balance unit.

Main experiments

Main experiments addressed possible area shrinking and volume loss of the glacier till the end of 21st century, as well as changes in the mass balance components.

Flow velocity

The maximum flow velocity on the surface of a considerably shrunk glacier dropped almost twice (Fig. 9) compared to the initial non-equilibrium state (Fig. 5). The area of maximum flow values in the elevation belt 4200–4270 m is located where ice thickness is also at the maximum, though the absolute figures do not exceed 20 m·yr^{-1}, that is twice lower compared to the beginning of experiments.

Topography and ice thickness

According to calculations, the glacier surface topography is in imbalance with the climate of 2014–2016. If the current surface air temperatures and precipitation will remain the same, the glacier will persistently shrink and lose 50 % of its volume and 40 % of its area by the end of the century (Fig. 4, *b*, *c*; 10, *a*, *b*); its right tributary will detach, and ice patches will persist at higher elevations. Both normal (E02) and accelerated (E01) scenarios predict ice thinning in the relatively gently sloping zone of 4200–4300 m asl, but shrinking in the latter is more prominent compared to E02 ice thickness paradoxically increases in the glacier part detached from the main body (Fig. 4, *a* and 4, *b*, *c*), possibly, as a consequence of the absence of dynamic mass redistribution. The glacier retreats 1600 m from the elevation about

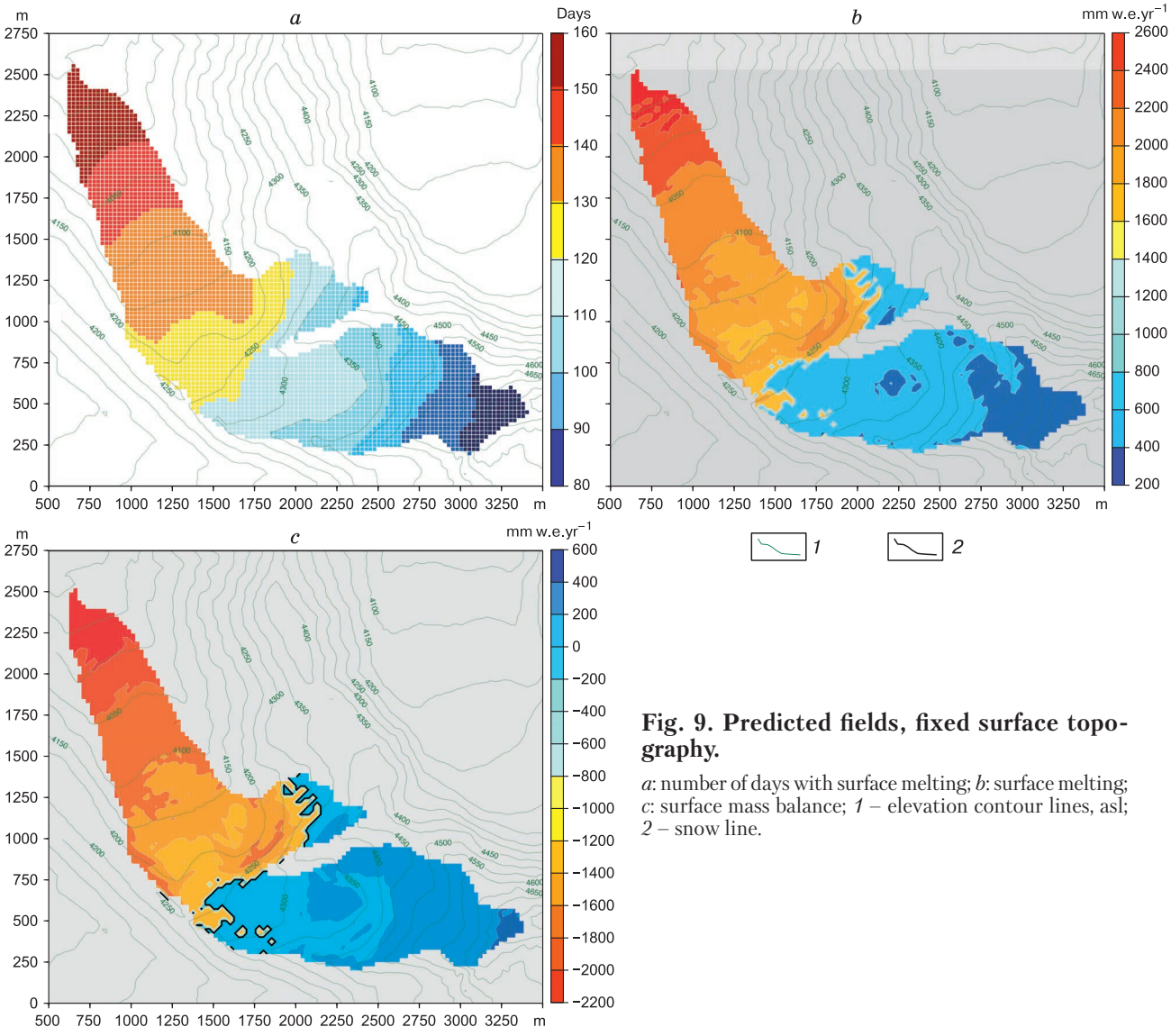

Fig. 9. Predicted fields, fixed surface topography.

a: number of days with surface melting; *b*: surface melting; *c*: surface mass balance; *1* – elevation contour lines, asl; *2* – snow line.

3900 m asl in the beginning of E01 and E02 to 4140–4150 m (E01, Fig. 4, *b*) and 4080–4100 m (E02, Fig. 4, *c*). Thus, the glacier will degrade even if the climate remains constant. Degradation will be especially rapid under condition of surface air temperature growth. According to the extreme scenario E10 (Fig. 4, *d*), it will disintegrate into two relatively large pieces (in the zone of thickest ice above 4600 m asl) and several smaller ice patches making up in total about 10 % of present area and 3 % of present volume (Fig. 10, *a*, *b*).

The decline is more rapid in the first 10 model years of E02 and slows down progressively to reach the steady state by the end of the experiment. During the first model decade, volumes and areas evolve at similar rates in all experiments because warming has not come into play yet (Fig. 10, *a*, *b*). In "odd" experiments, at higher surface flow velocities, the first decade of rapid shrinking is followed by a period of relative stability while the volume keeps reducing. The duration of this period decreases at higher warming rates.

Precipitation and runoff

The growth of air temperature in experiments E07–E10 leads to initial increase in liquid precipitation which decreases subsequently by the factor from 2 to 6 (Fig. 10, *c*) while the glacier retreats and its lower parts melt out, where the temperature is higher Note, that results of calculations are presented as absolute values. The share of rain in the runoff increases from 9 to 9.5–11.5 % and then decreases to below the initial value in experiments E04–E10 (Fig. 10, *d*). Both total (Fig. 10, *e*) and glacial (Fig. 10, *f*) runoff reduces in all experiments. The rate of reduction is similar in the first model decade. Note that runoff de-

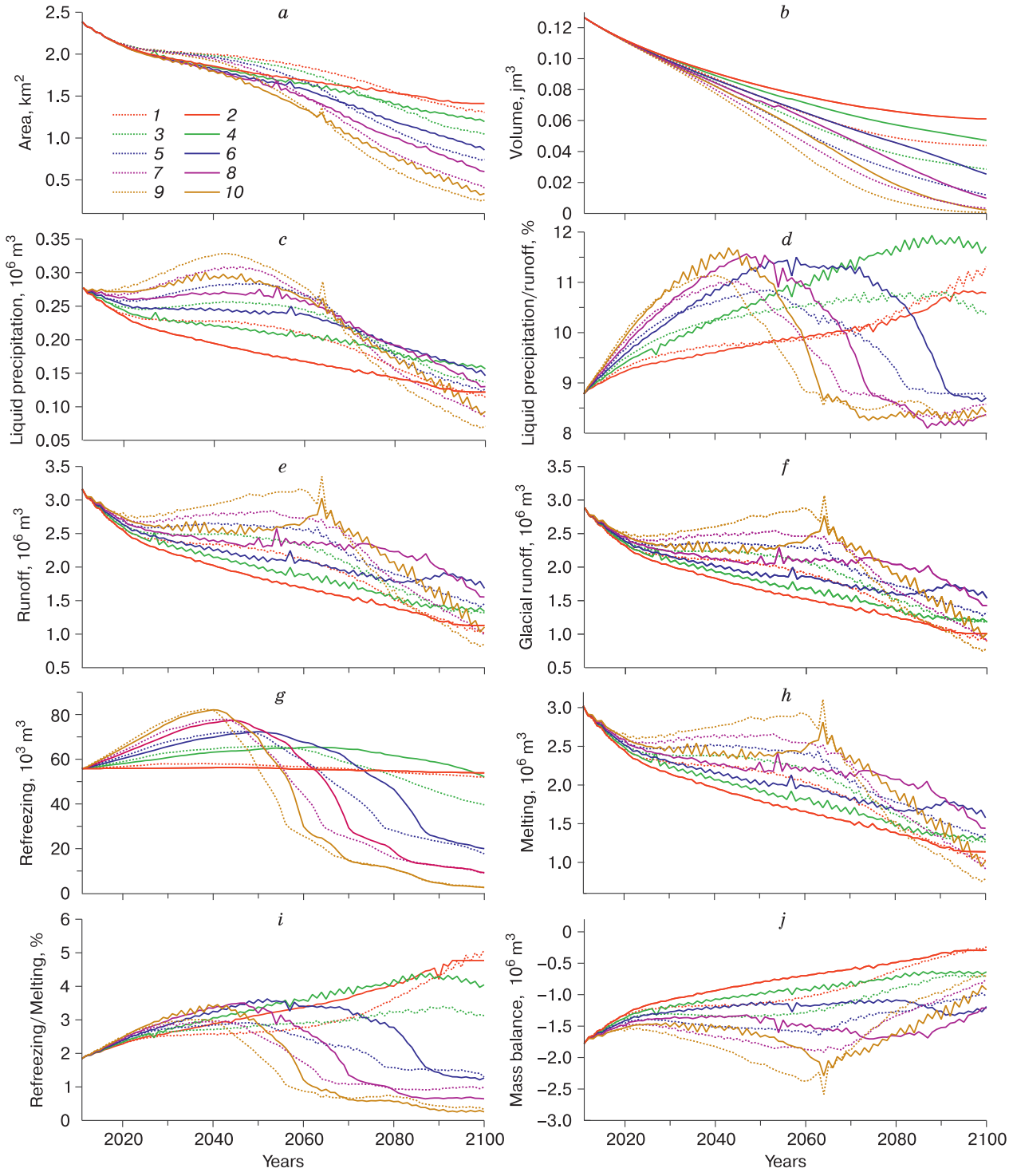

Fig. 10. Summary of numerical experiments: evolution of characteristics of Sary-Tor glacier during 90 model years:

a: glacier area; *b*: ice volume; *c*: volume of liquid precipitation; *d*: fraction of liquid precipitation in total runoff volume; *e*: total runoff volume; *f*: glacial runoff volume; *g*: internal feeding (refrozen meltwater); *h*: meltwater volume; *i*: fraction of refreezing in meltwater volume; *j*: surface mass balance; *1* to *10* are experiment numbers.

creases systematically in experiments E01–E04 when the temperature either remains constant or grows insignificantly (1 °C/100 yr). In other experiments and in some time periods, the runoff shows a more or less prolonged increase: after the year 2080 in E06 and after 2020 in E09; in the latter case, it keeps increasing for the following 40 years and falls abruptly after a peak at 2062 when it exceeds the initial value. Similarly, but not as extremely, runoff evolves in experiment E10 and grows slightly faster in E07, possibly due to more rapid melting (Fig. 10, *h*). Glacial runoff decreases after the glacier and its ablation zone become smaller. We cannot exclude that the main runoff changes may occur at the peak of melting season (July–August), when the runoff grows with respect to the present annual sum. However, this issue requires special investigation.

The period of stable runoff is minor or absent in experiments E01–E06. For instance, both total and glacial runoff systematically decreases in experiment E02 (conventional present-day climate).

Melting and refreezing

Pattern of surface melting is similar to that of runoff (Fig. 10, *h*). Refrozen meltwater volume (roughly corresponding to a somewhat broader concept of internal feeding [*Golubev et al., 1978*]) remains almost invariable in experiments E01 and E02 but its ratio to the volume of meltwater changes substantially (Fig. 10, *i*) and depends on a particular climatic scenario: the ratio increases from 2 to 5 % in E01–E04 but decreases from 0.1–0.2 % in E09 and in E10 to 0.16–0.17 % in E04 and E05. Refrozen water extent is limited to the area where snow cover remains during ablation season. This area reaches stable minimum size in experiments E05–E10, which explains stability of refrozen water volume since some point in time.

Surface mass balance

The evolution pattern of the integral indicator, surface mass balance, is actually reverse to the runoff and melting patterns (Fig. 10, *j*). It persistently increases in experiments E01–E04, In "extreme" experiments, E09 and E10, surface mass balance decreases till the year 2060 and next grows again. Other scenarios predict of minor increase and decrease.

Results of numerical experiments should not be accepted as a forecast for particular years. Interannual variability of precipitation and surface air temperature, and, therefore, variability of melting rate is rather high. The model assimilates conventional mean climatic values, which reflect only global trends, not interannual variability. Accordingly, prognostic calculations aim at revealing general tendencies in glacier evolution. Examination of interannual variability influence on projections of mass balance components requires separate study.

CONCLUSIONS

The study aimed at elucidating methodological problems of glacier evolution using mathematical modeling. Model structure and set-up of numerical experiments were considered and results of simulations were analyzed. Following conclusions can be formulated:

1. Sary-Tor glacier is in imbalance with the present climate and may reach equilibrium in a few decades. If the climate remains constant, volume and area of the glacier will reduce substantially during 90 model years (more than 40 % in area and more than 50 % in volume). Its front is expected to retreat by approximately 1600 m.

2. Under gradual surface air temperature growth, the glacier persistently degrades. In case of temperature increase at the rate of 4 °C/100 yr, the glacier will disintegrate in several fragments of approximately 10 % in area and 3 % in volume of the initial values.

3. If air temperature will increase at the rate of 2–4 °C/100 yr, ratio of liquid precipitation will increase from 9 to 11 %. The ratio will drop below the initial level after the year 2040 because of contraction of glaciated area.

4. Glacial runoff decreases by the year 2100 in all numerical experiments. In case present climate conserved, runoff volume will decrease twice. However, air temperature growth at the rate 1–3 °C/100 yr will cause slowdown of runoff decrease caused by high melting rate. In case of temperature at the rate 4 °C/100 yr, decrease in runoff volume will be additionally controlled by significantly shrinkage of the glacier area.

5. If the present climate conditions persist, surface mass balance of the glacier will increase gradually and will stabilize by the year 2100, when the glacier will approach equilibrium) with the present climate (however, it will not be completely equilibrated).

Since Sary-Tor may be conventionally accepted as a reference glacier for Ak-Syirak Massif, its future state may be extrapolated on other glaciers in the region.

Authors thank Kumtor Gold Company for financial and logistic support of the Program of monitoring glaciers and hydrometeorological observations on the concession territory of Kumtor Gold Company in Arabel and Uchkol river basins. Authors also appreciate anonymous reviewers for valuable comments and suggestions, which allowed to substantially improve initial manuscript of the paper.

The research was carried out within the frameworks of the Program of basic research of Presidium of RAS No. 52 "Providing sustainable development of the South of Russia under climatic, ecologic and technogenic challenges" (sub-program "Developing resource

potential, retention of the leadership positions and providing security of the Black Sea and Caspian Regions on the basis ecosystem principles").

References

Aizen, V.B., Aizen, E.M., Kuzmichonok, V.A., 2007. Glaciers and hydrological changes in the Tien Shan: simulation and prediction. Environ. Res. Lett. 2, p. 045019, DOI: 10.1088/1748-9326/2/4/045019.

ASTER Global Digital Elevation Map [Electronic resource]. – URL: https://asterweb.jpl.nasa.gov/gdem.asp (submittal date: 10.02.2015).

Baetov, B.I., Arkhangelskaya, A.V., 2015. Change in river runoff and its challenge to hydropower security. Vestnik KRSU 15 (1), 140–143.

Barandun, M., Huss, M., Usubaliev, R., et al., 2018. Multi-decadal mass balance series of three Kyrgyz glaciers inferred from modelling constrained with repeated snow line observations. The Cryosphere, 12, 1899–1919, DOI: https://doi.org/10.5194/tc-12-1899-2018.

Bernauer, T., Siegfried, T., 2012. Climate change and international water conflict in Central Asia. J. Piece Res. 49, 227–239, DOI: 10.1177/0022343311425843.

Bolch, T., 2007. Climate change and glacier retreat in northern Tien Shan (Kazakhstan/Kyrgyzstan) using remote sensing data. Global and Planet. Change 56, 1–12.

Braithwaite, R.J., Olesen, O.B., 1990. A simple energy-balance model to calculate ice ablation at the margin of the Greenland ice sheet. J. Glaciol. 36, 222–228.

Dozier, J., Frew J., 1990. Rapid calculation of terrain parameters for radiation modeling from digital elevation data. IEEE Trans. on Geosci. and Remote Sensing 28 (5), 963–969.

Duyrgerov, M., 2010. Reanalysis of glacier changes: from the IGY to the IPY, 1960–2008. Data of Glaciol. Studies, issue 108, 6–115.

Duyrgerov, M.B., Kunahovich, M.G., Mikhalenko, V.N., et al., 1992. Mass balance, runoff and meteorological conditions of Sary-Tor glacier in Ak-Shiyrak crest (Inner Tien Shan). Izdvo RAN, Moscow, 70 pp. (in Russian)

Duyrgerov, M.B., Ushnurtsev, S.N., 1988. Mass balance of Sary-Tor glacier. Materialy Glyaciologicheskih Issledovanii (Data of Glaciological Studies), No. 62, 199–203.

Duyrgerov, M.B., Ushnurtsev, S.N., Chichagov, A.M., 1991. Links between elevation of feeding boundary, air temperature and runoff in the basin of Sary-Tor glacier, Inner Tien Shan. Materialy Glyaciologicheskih Issledovanii (Data of Glaciological Studies), No. 71, 136–139.

Golubev, G.N., Duyrgerov, M.B., Markin, V.A., et al., 1978. Djankuat Glacier (Central Caucasus). Water, ice and heat balance of mountain glaciers basins. Gidrometeoizdat, Leningrad, 183 pp. (in Russian)

Fürst, J.J., Rybak, O., Goelzer, H., et al., 2011. Improved convergence and stability properties in a three-dimensional higher-order ice sheet model. Geosci. Model Development 4, 1133–1149, DOI: 10.5194/gmd-4-1133-2011.

Hagg, W., Mayer, C., Lambrecht, A., Helm, A., 2008. Sub-debris melt rates on southern Inylchek Glacier, central Tian Shan. Geografiska Annal. 90A, 55–63.

Huss, M., Hock, R., 2018a. A new model for global glacier change and sea-level rise. Frontiers in Earth Science [Electronic resource]. – URL: https://www.frontiersin.org/articles/10.3389/feart.2015.00054/full 2015, vol. 3, Article 54, DOI: 10.3389/feart.2015.00054 (submittal date: 01.10.2018).

Huss, M., Hock, R., 2018b. Global-scale hydrological response to future glacier mass loss. Nature Climate Change 8, 135–140, DOI: 10.1038/s41558-017-0049-x.

Ibatullin, S., Yasinsky, V., Mironenkov, A., 2009. The impact of climate change on water resources in Central Asia. Sector report No. Almaty, Rep. Kazakhstan, Eurasian Development Bank, 43 pp.

Janssens, I., Huybrechts, P., 2000. The treatment of meltwater retention in mass-balance parameterizations of the Greenland ice sheet. Ann. Glaciol. 31, 133–140.

Kenzhebaev, R., Barandun, M., Kronenberg, M., et al., 2017. Mass balance observations and reconstructions for Batysh Sook Glacier, Tien Shan, from 2004 to 2016. Cold Regions Sci. and Technol. 135, 76–89, DOI: https://doi.org/10.1016/j.coldregions.2016.12.007.

Kondratiev, K.Ya., 1965. Actinometry. Gidrometeoizdat, Leningrad, 695 pp. (in Russian)

Kronenberg, M., Barandun, M., Hoelze, M., et al., 2016. Mass-balance reconstruction for Glacier No. 354, Tien Shan, from 2003 to 2014. Ann. Glaciol. 57. 92–102, DOI: 10.3189/2016AoG71A032.

Kutuzov, S., Shahgedanova, M., 2009. Glacier retreat and climatic variability in the eastern Terskey-Alatoo, inner Tien Shan between the middle of the 19th century and beginning of the 21st century. Global and Planet. Change 69, 59–70.

Kuzmichenok, V.A., 1988. Variations of Davydova and Sary-Tor glaciers from the data of topographic surveys. Materialy Glyaciologicheskih Issledovanii (Data of Glaciological Studies), No. 62, 193–198.

Lutz, A.F., Immerzeel, W.W., Shrestha, A.B., Bierkens, M.F.P., 2014. Consistent increase in High Asia's runoff due to increasing glacier melt and precipitation. Nature Climatic Change 4, 587–592.

Mikhalenko, V.N., 1993. Calculation and reconstruction of mass balance of the ice system Akshiyrak in the Tien Shan. Materialy Glyaciologicheskih Issledovanii (Data of Glaciological Studies), No. 76, 102–107.

Morozova, P.A., Rybak, O.O., 2017. Downscaling of the global climate model data for the mass balance calculation of mountain glaciers. Led i Sneg (Ice and Snow) 57 (4), 437–452, DOI: 10.15356/2076-6734-2017-4-437-452.

Nemec, J., Huybrechts, P., Rybak, O., Oerlemans, J., 2009. Reconstruction of the surface mass balance of Morteratschgletscher since 1865. Ann. Glaciol. 50, 126–134.

Oerlemans, J., 1991. The mass balance of the Greenland ice sheet: sensitivity to climate change as revealed by energy-balance modeling. The Holocene 1, 40–49.

Oerlemans, J., 2001. Glaciers and Climate Change. A.A. Balkema Publ., Rotterdam, 148 pp.

Oke, T.R., 1987. Boundary layer climates. Second edition. Tailor & Fransis, Oxford, UK, 435 pp.

Pattyn, F., 2003. A new three-dimensional higher-order thermomechanical ice sheet model: Basic sensitivity, ice stream development, and ice flow across subglacial lakes. J. Geophys. Res. 108, 2382, DOI: 10.1029/2002JB002329.

Petrakov, D.A., Lavrentiev, I.I., Kovalenko, N.V., Usubaliev, R.A., 2014. Ice thickness, volume and current changes of the Sary-Tor glacier area (Ak-Shiyrak Massif, Inner Tien Shan). Earth's Cryosphere XVIII (3), 83–91.

Petrakov, D., Shpuntova, A., Aleinikov, A., et al., 2016. Accelerated glacier shrinkage in the Ak-Shyirak massif, Inner Tien Shan, during 2003–2013. Science of the Total Environ. 562, 364–378, DOI: http://dx.doi.org/10.1016/j.scitotenv.2016.03.162.

Popovnin, V.V., Pylaeva, T.V., 2015. Avalanche feeding of the Djankuat glacier. Led i Sneg (Ice and Snow) 55 (2), 21–32, DOI: https://doi.org/10.15356/2076-6734-2015-2-21-32.

Reijmer, C.H., van den Broeke, M.R., Fettweis, X., et al., 2012. Refreezing on the Greenland ice sheet: a comparison of parameterizations. The Cryosphere 6, 743–762.

Rets, E.P., Frolova, N.L., Popovnin, V.V., 2011. Modeling of melting on the surface of a mountain glacier. Led i Sneg (Ice and Snow) 51 (4), 24–31.

Robinson, A., Calov, R., Ganopolski, A., 2010. An efficient regional energy-moisture balance model for simulation of the Greenland Ice Sheet response to climate change. The Cryosphere 4, 129–144.

Rybak, O.O., 2011. Mathematical modeling of evolution of ice sheets. Fizmatlit, Moscow, 220 pp. (in Russian)

Rybak, O.O., Rybak, E.A., 2017. Implementation of observations at regular meteorological stations for mass balance calculation of mountain glaciers (case study of Djankuat glacier, Central Caucasus). Systems of the Environmental Control, No. 9 (29), 100–108. (in Russian)

Rybak, O.O., Rybak, E.A., Kutuzov, S.S., et al., 2015. Calibration of a mathematical model of Marukh glacier, Western Caucasus. Led i Sneg (Ice and Snow) 55 (2), 9–20, DOI: https://doi.org/10.15356/2076-6734-2015-2-9-20.

Siegfried, T., Bernauer, T., Guinnet, R., et al., 2012. Will climate change exacerbate water stress in Central Asia? Climatic Change 112, 881–899, DOI: 10.1007/s10584-011-0253-z.

Sorg, A., Bolch, T., Stoffel, M., et al., 2012. Climate change impacts on glaciers and runoff in Tien Shan (Central Asia). Nature Climate Change 2, 725–731, DOI: 10.1038/nclimate1592.

Ushnurtsev, S.N., 1991. Oscillations of mass balance of Sary-Tor glacier in the Inner Tien Shan and its reconstructions for the years 1930–1988. Materialy Glyaciologicheskih Issledovanii (Data of Glaciological Studies), No. 71, 70–80.

Voloshina, A.P., 2002. Meteorology of mountain glaciers. Materialy Glyaciologicheskih Issledovanii (Data of Glaciological Studies), No. 92, 3–148.

Zekollari, H., Fürst, J.J., Huybrechts, P., 2014. Modelling the evolution of Vadret da Morteratsch (Switzerland) since the Little Ice Age and into the future. J. Glaciol. 60, 1155–1168, DOI: 10.3189/2014JoG14J05363A434.

Zekollari, H., Huybrechts, P., Fürst, J.J., et al., 2013. Calibration of a higher-order 3D ice flow model of the Morteratsch glacier complex, Engadin, Switzerland. Ann. Glaciol. 54, 343–351, DOI: 10.3189/2013AoG63A434.

Zekollari, H., Huybrechts, P., Noël, B., et al., 2017. Sensitivity, stability and future evolution of the world's northernmost ice cap, Hans Tausen Iskappe (Greenland). The Cryosphere 11, 805–825, DOI: 10.5194/tc-11-805-2017.

Received May 7, 2018
Revised version received December 10, 2018
Accepted January 10, 2019